

Numerical simulations of inviscid three-dimensional flows at single- and dual-pump intakes

Simulation numériques des écoulements non-visqueux tridimensionnels dans un bassin d'aspiration d'une station de pompage avec une seule pompe, et avec des pompes doubles

MATAHEL ANSAR, *Senior Civil Engineer, South Florida Water Management District, 3301 Gun Club Road, West Palm Beach, FL 33406 USA*

TATSUAKI NAKATO, *Associate Director, Iowa Institute of Hydraulic Research, The University of Iowa, Iowa City, IA 52242 USA*

GEORGE CONSTANTINESCU, *Post-Doctoral Research Fellow, Center for Turbulence Research, Building 500, Stanford University, Stanford, CA 94305-3030 USA*

ABSTRACT

Three-dimensional inviscid solutions for pump-approach flow distributions within both a single-pump and a dual-pump sump model were developed. The single-pump sump model consisted of a rectangular pump bay with a vertical circular pipe located at the downstream end of the bay. The two-pump sump model consisted of a wider rectangular pump bay with two vertical circular pipes located at the downstream end of the bay. The equations of motions were solved in generalized curvilinear coordinates on a non-staggered grid. For the single-pump model, the simulations were carried out for two cases, cross-flow and no-cross-flow. The results are in good agreement with laboratory flow measurements obtained from a 1:10-scale model using an Acoustic Doppler Velocimeter. For the two-pump sump model, simulations were also carried out for two cases. In Case 1, an equal pumping discharge was delivered through the two pipes, and in Case 2 the total discharge was split in a 7-to-3 ratio between the two pipes. The results for the two cases were compared with a focus on the formation of free-surface and subsurface vortices surrounding the pumps.

RESUMÉ

Des solutions tridimensionnelles ont été obtenues pour un écoulement non visqueux dans une station de pompage avec une seule pompe, et puis avec deux pompes. La station de pompage avec une seule pompe consiste d'un bassin d'aspiration rectangulaire et d'une conduite circulaire et verticale située à l'extrémité aval du bassin. La station de pompage avec deux pompes consiste d'un plus grand bassin d'aspiration rectangulaire et de deux conduites circulaires et verticales situées à l'extrémité aval du bassin. Les équations sont résolues en utilisant un système de coordonnées curvilinéaires sur un maillage colloqué. Pour la station de pompage avec une seule pompe, les simulations numériques sont obtenues pour deux cas, avec un écoulement latéral, et sans écoulement latéral. Les résultats numériques sont en accord avec des mesures d'écoulement obtenus au laboratoire avec une maquette à petite échelle. Pour la station de pompage avec deux pompes, les simulations ont aussi été obtenues pour deux cas. Dans le premier cas, le débit total qui alimente la station est réparti également entre les deux conduites, et dans le deuxième cas le débit total est réparti en une proportion de 7 à 3 entre les deux conduites. Les résultats des deux cas sont comparés avec un accent particulier sur les différences enregistrées dans la distribution et l'intensité des différents tourbillons qui forment à la surface libre ou des tourbillons submergés originant près des parois du bassin d'aspiration.

1 Introduction

When a pump intake bay is not properly designed, severe swirling flow problems may occur in the pump bay. Particularly, a swirling flow occurs when pump-approach flow distributions within the intake bay are not uniform regardless of its origin. In the case of a single-pump bay, existence of cross flow outside the intake may cause severe flow separation at the intake entrance, resulting in swirling flow conditions (Nakato 1984; Ansar and Nakato 1995; Nakato and Krütten 1999). In the case of a pump intake with multiple pumps, swirling flow may be produced by uneven pump capacities even if there is no cross flow in front of the intake (Bauer et al. 1997). Swirling flow, in general, results in uneven impeller loading as well as formation of free-surface and subsurface vortices, all of which are detrimental for proper pump operations. Common pump-operating problems, such as impeller cavitation, bearing wear, noise and vibration problems, are often caused by swirling flows.

Traditionally, small-scale laboratory models are used to solve these problems using flow-straightening devices, such as baffle bars and perforated plates to rectify nonuniform pump-approach flow conditions, as well as vortex-suppressing devices, such as floor and backwall-attached splitters (Tullis 1979; Sweeney et al. 1982; Melville et al. 1994; Bauer et al. 1997). However, pump-related problems are often site specific and different solutions are needed for each site. Because of the costs involved in the design and operation of small-scale laboratory models, there is a need for more research in the numerical simulations of pump-approach flow distributions and vortex formation at water intakes.

The present paper describes a detailed solution for the three-dimensional inviscid flow in rectangular pump bays with one pump and two pumps. Turbulent flow calculations for the single-pump intake were carried out by Constantinescu and Patel (1997) using $k-\varepsilon$ and $k-\omega$ turbulence models. An inviscid solution was considered in this study because upstream vorticity at a typical water intake is convected through the pump bay and re-organizes into

Revision received March 23, 2001. Open for discussion till December 31, 2002.

free-surface and subsurface vortices near the suction pipe through an essentially inviscid process, i.e., amplification of vorticity by stretched vortex filaments. The purpose of the present work is to determine the accuracy and reliability of the inviscid solution in predicting pump-approach flow features at a single-pump intake. It is also intended to investigate the formation of free-surface and subsurface vortices near the intake suction pipes in single and two-pump intakes.

For the single-pump model, the numerical simulations were carried out for both cross-flow and no-cross-flow cases and the results were compared with experimental data obtained by Ansar (1997). The results showed a good agreement with laboratory flow measurements, which motivated numerical model extension to a two-pump sump geometry. The two-pump sump model simulations were carried out for two cases: in Case 1, an equal pumping discharge was delivered through the two pipes, and in Case 2, the total discharge was split in a 7-to-3 ratio between the two pipes.

This paper describes the numerical method, comparisons of the single-pump flow simulations with experiments, and the results for the two-pump intake with a focus on the formation of free-surface and subsurface vortices surrounding the pumps.

2 Numerical Method

The numerical method used was based on the one developed by Sotiropoulos and Patel (1992) and Constantinescu and Patel (1997). Several modifications were implemented for the pump intake geometry including handling of the geometry using multi-block techniques (Constantinescu and Patel 1997).

2.1 Equations in Generalized Curvilinear Coordinates

The governing equations were written in generalized curvilinear coordinates (ξ^1, ξ^2, ξ^3) in order to accurately solve the flow in the complex-geometry computational domain of a water intake. This was achieved by applying a partial transformation where the independent variables x_i are transformed to ξ^i , but leaving the velocity components U_i in cartesian coordinates. The governing equations for the continuity and the momentum equations thus transformed are as follows (Sotiropoulos and Patel 1992):

(i) Continuity Equation

$$\frac{1}{J} \frac{\partial}{\partial \xi^i} (JU^i) = 0 \quad (1)$$

where J is the Jacobian of the geometric transformation $(x^1, x^2, x^3) \rightarrow (\xi^1, \xi^2, \xi^3)$ and U^i are the contravariant components of velocity.

(ii) Momentum Equation

$$\frac{\partial \vec{Q}}{\partial t} + A_j \frac{\partial \vec{Q}}{\partial \xi^j} + \vec{H} = 0 \quad (2)$$

In the above equations, \vec{Q} is the velocity vector defined by $\vec{Q} = (U_1, U_2, U_3)^T$ in cartesian coordinates. The matrices A_j in the convective terms are diagonal matrices defined as follows:

$$A_j = \text{diag}(U^j, U^j, U^j) \quad (3)$$

where U^j are the contravariant components of velocity. \vec{H} are the gradient terms for pressure, P , and are given by

$$\vec{H} = \left(\frac{\partial P}{\partial \xi^k} \xi_{x_1}^k, \frac{\partial P}{\partial \xi^k} \xi_{x_2}^k, \frac{\partial P}{\partial \xi^k} \xi_{x_3}^k \right)^T \quad (4)$$

2.2 Numerical Solution of the Governing Equations

The momentum equations were discretized in space, on a non-staggered mesh, using three-point central finite differencing for the pressure gradient, and second order upwind finite differencing for the convective terms. The continuity equation was discretized using three-point central differences. The discrete momentum equations were integrated in time using a four-stage ($m = 1$ to 4), explicit Runge-Kutta scheme. The discrete momentum equations were substituted in the discrete continuity equation to obtain a Poisson equation for the pressure field at the intermediate stage ($m-1$). The pressure Poisson equation was then solved using the Alternate Direction Implicit (ADI) method. The convergence rate of the time marching procedure was enhanced by employing local-time stepping techniques along with implicit residual smoothing. The details of this procedure are given by Sotiropoulos and Patel (1992) and Constantinescu et al. (1997).

2.3 Boundary Conditions

A known velocity profile was imposed at the upstream end of the approach channel. At all solid boundaries, a slip boundary condition was used and at the free surface, a symmetry boundary condition was used. At the outlet of the suction pipe, the zero second-derivative condition was applied to the axial velocity. For the slip boundary condition, Von Neumann condition, i.e., the no-penetration condition, was used at solid walls, i.e.,

$$\frac{\partial \vec{U}}{\partial \vec{n}} = \vec{U} \cdot \vec{n} = 0 \quad (5)$$

where \vec{U} is the velocity vector and \vec{n} is the unit normal vector to the wall.

3 Single-Pump Intake

3.1 The Computational Grid

The computational grid for the single-pump intake is depicted in Fig. 1. The grid consists of two blocks: Block 1, representing the rectangular channel and the submerged portion of the suction pipe, has 63x46x27 grid points in the x , y , and z directions, respectively; and Block 2, representing the portion of the suction

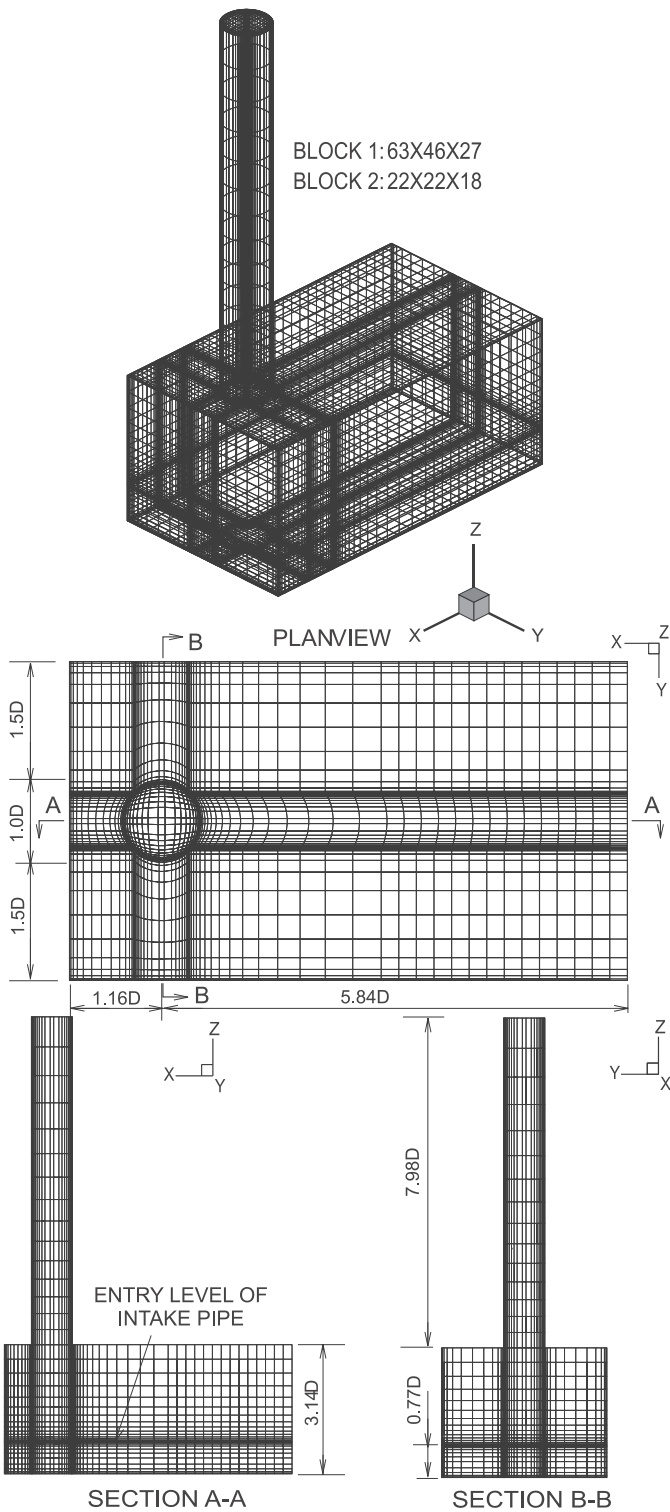


Fig. 1 Computational grid for the single-pump intake

pipe above the free surface, has $18 \times 18 \times 16$ grid points in the x , y , and z directions, respectively. Systematic grid refinement studies, carried out by the first author (Ansar 1997), showed that this mesh density is sufficient for grid independent solutions. The geometrical characteristics of this intake are the same as those of the single-pump intake model used in the laboratory experiments to validate the numerical solutions. The geometrical characteristics in question are the ratios of backwall, sidewall, and floor clearances to the diameter of the suction pipe, and the ratio of the

submergence depth to the diameter of the suction pipe.

3.2 Comparisons with Experiments

Prior to comparing the numerical results to the experimental measurements, convergence tests of the numerical solution were carried out. The convergence for the inviscid flow solution was evaluated by looking at the time-history of the convergence of the solution, and by comparing the results at different numbers of iterations. Convergence was achieved at 15,000 iterations and beyond (Ansar 1997).

The results of the inviscid solution in the single-pump intake were compared with the experimental results described in Ansar (1997) and Ansar and Nakato (2001). In these experiments, three-dimensional measurements of the velocity field were obtained with an Acoustic Doppler Velocimeter at eleven sections within the pump sump, namely Sections A through K, as shown in Fig. 2. At each section, velocity measurements were obtained at eleven verticals and at eight equally-spaced locations along each vertical. Experiments were conducted for two cases. In the first case, there was no cross-flow upstream of the pump bay, i.e., the pump-approach flow was directly supplied to the intake bay with no flow diversion. In the second case, there was a strong cross-flow upstream of the pump bay, i.e., the intake flow was withdrawn from the main channel into the intake bay at a right angle. In this case, one-eighth of the total discharge in the main channel was diverted to

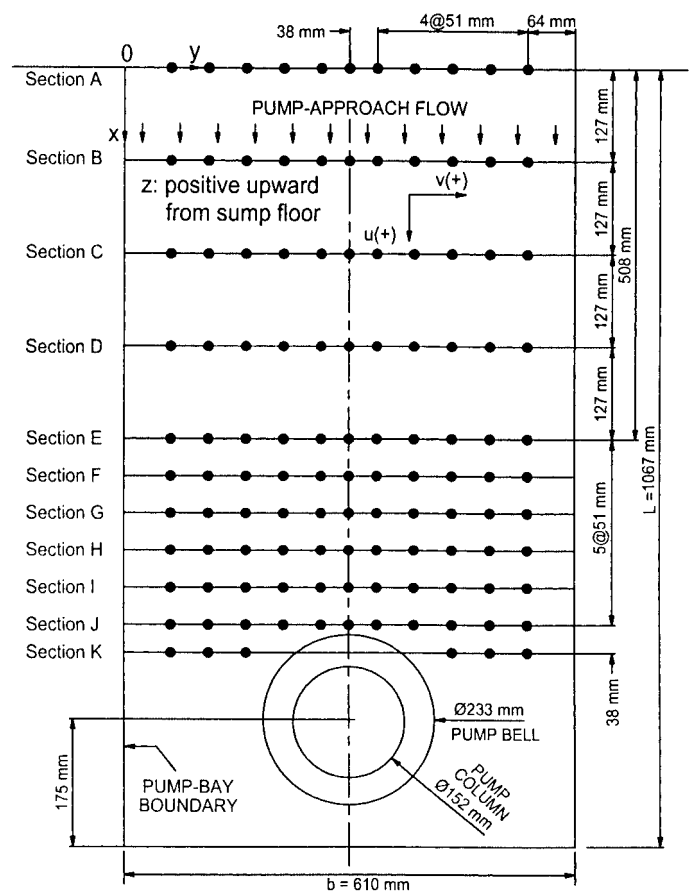


Fig. 2 Locations of verticals where three-dimensional velocity data were obtained

the intake bay. The approach flow conditions are summarized in Table 1. In Table 1, h is the depth of the approach flow, b is the width of the pump sump, g is the acceleration of gravity, and ν is the kinematic viscosity of water. The values of these parameters are given in Table 1. In both the no-cross-flow and cross-flow cases, the measured velocity distributions at Section B were taken as the upstream boundary conditions because the measurements at Section A were extremely unstable and had more uncertainties.

Table 1: Summary of the approach flow conditions

Flow Condition	Total Discharge in Main Channel Q_{main} (l/s)	Pump-Intake Discharge Q (l/s)	Froude Number for Pump-Approach Flow $Fr = \frac{Q}{bh\sqrt{gh}}$	Reynolds Number for Pump-Approach Flow $Re = \frac{Q}{\nu h}$
No Cross-Flow	0.0	14.0	0.022	30,700
Cross-Flow	113.0	14.0	0.022	30,700

Note: Pump-sump width, $b = 61.0$ cm; Suction-line floor clearance, $c = 11.8$ cm; Suction-pipe diameter, $D = 15.2$ cm; Pump-approach flow depth, $h = 47.9$ cm; and Kinematic viscosity, $\nu = 0.00952$ cm²/s at temperature $T = 22.2$ °C

3.2.1 Flow patterns

Comparison of the flow patterns observed from experiments and those predicted by the inviscid solution at $z = 2.5D$ for the no-cross-flow case are shown in Fig. 3 in which z is the vertical coordinate measured from the sump floor, D is the diameter of the suction pipe, and $z = 3.14D$ is at the free surface. Fig. 3(a) depicts the flow patterns observed in the experiments, including two intermittent free-surface vortices, V_1 and V_2 . These vortices, and their directions of rotation, are predicted by the inviscid solution, as shown in Fig. 3(b). The free-surface vortices, predicted by the numerical solution, although not intermittent, are not always stationary. This is because the position of each core can shift slightly when the simulations are carried out for a significant additional number of iterations (about 3,000 additional iterations).

Fig. 4 shows a comparison of flow patterns observed from experiments and those predicted by the inviscid solution at $z = 2.5D$ for the cross-flow case. The main flow features in this case are shown in figure 4(a), including a large re-circulation zone in the approach channel, a strong counterclockwise vortex located between the suction pipe and the left sidewall (vortex V_1), and a weak clockwise vortex located between the suction pipe and the right sidewall (vortex V_2). Fig. 4(b) shows that the large re-circulation region, including its direction of rotation, the two free-surface vortices, and the high streamwise velocities near the left wall, are predicted by the inviscid solution. However, the core of the re-circulation zone is shifted toward the longitudinal axis of symmetry of the sump. The relative positions of the vortices are also different from those observed in the experiments.

The re-circulation region in the cross-flow case forms in the pump bay because of convection and re-organization of strong

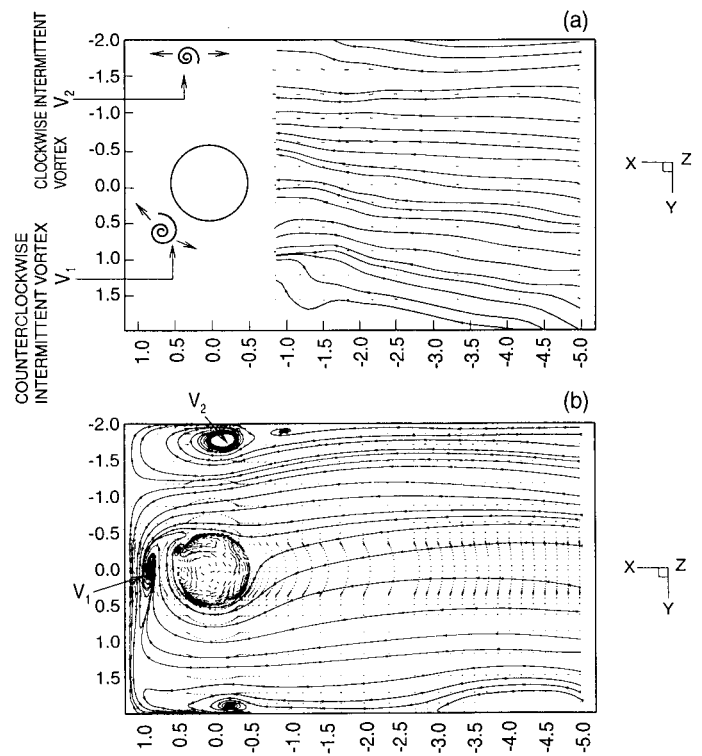


Fig. 3 Flow patterns at $z = 2.5D$ in no cross-flow case: (a) Experiments and (b) Inviscid solution

vorticity induced by a highly spatially non-uniform flow at the entrance of the intake. The vortices near the intake pipe form because of the amplification of the convected vorticity through vortex-filament stretchings.

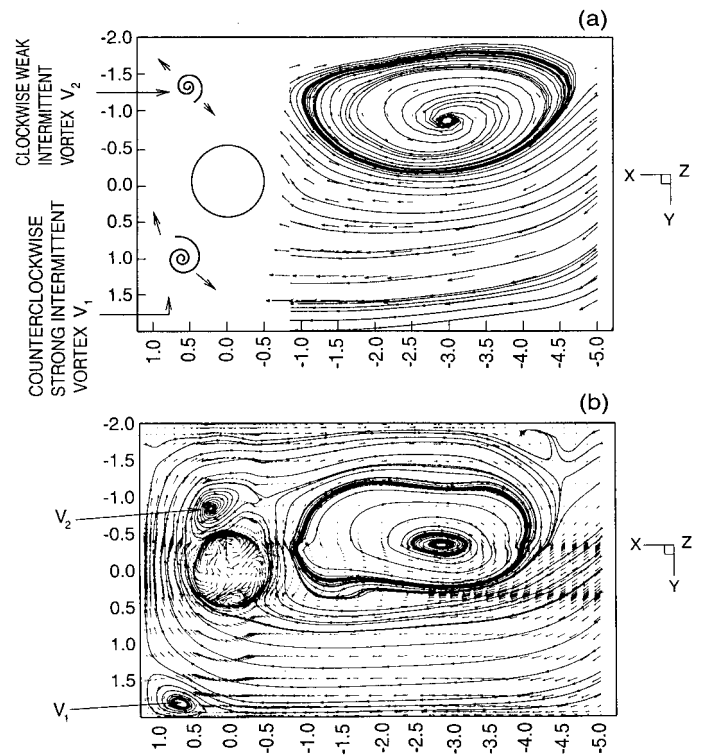


Fig. 4 Flow patterns at $z = 2.5D$ in cross-flow case: (a) Experiments and (b) Inviscid solution

3.2.2 Streamwise velocity distributions

Comparisons of the transverse distributions of the streamwise velocity for the no-cross-flow experiments and the inviscid solution at $z/h = 0.4$ are shown in Fig. 5. In this figure, h is the depth of the approach flow, y is the transverse distance measured from the longitudinal axis of symmetry of the intake. Note that $y/D = 2$ and $y/D = -2$ are located at the left and the right sidewalls, respectively. The streamwise velocity, U , was normalized by the mean axial velocity in the suction pipe, U_p . The comparisons were carried out at Sections B through J. These results show a good agreement between the no-cross-flow experiments and the inviscid solution, particularly at Sections E, F, and G.

Comparisons of the transverse distributions of the streamwise velocity for the cross-flow experiments and the inviscid solution at $z/h = 0.4$ are shown in Fig. 6. Fig. 6 shows a good agreement between the cross-flow experiments and the inviscid solution. The streamwise velocities at all sections are particularly well predicted in the region of high positive velocities near the left sidewall at $y/D = 2.0$. The reverse flow region near the right sidewall is also predicted. The experimental data at Section D fall exactly on the inviscid solution curve. At other sections, the experimental data are either on the inviscid solution curve or very close to it. Except for very low velocity regions near $y/D = 0.0$, the percent difference between the cross-flow experiment and the inviscid solution was less than 6 percent. This level of agreement is close to the 3 percent accuracy of the ADV measurements obtained in the uncertainty analysis of the ADV data (Ansar 1997).

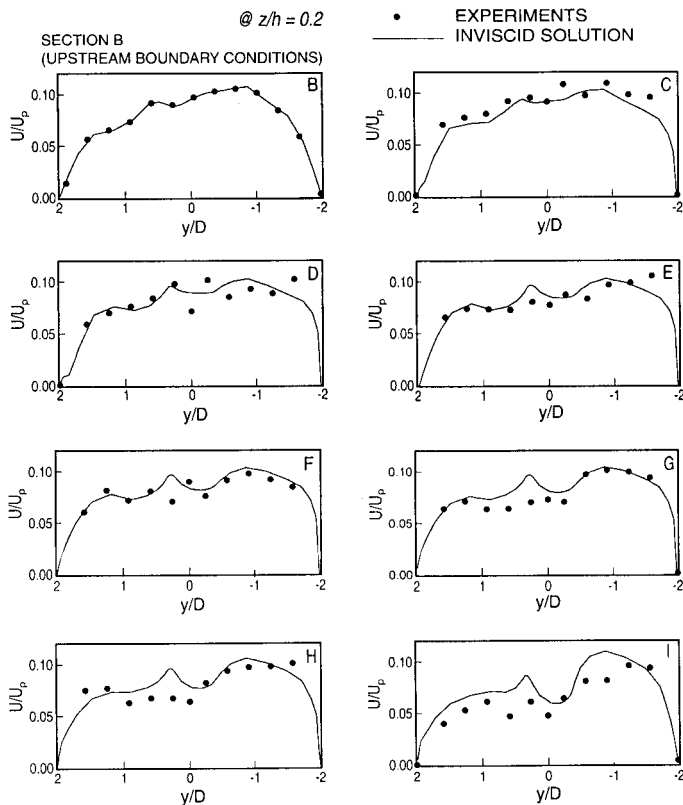


Fig. 5 Comparison of inviscid solution and experimental data: transverse distributions of streamwise velocity at $z/h = 0.2$ without cross flow

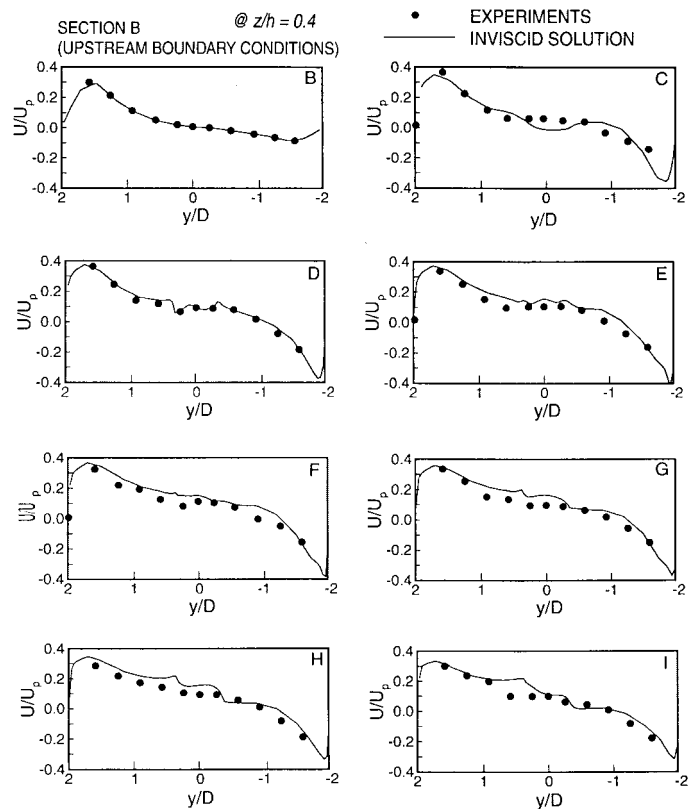


Fig. 6 Comparison of inviscid solution and experimental data: transverse distributions of streamwise velocity at $z/h = 0.4$ with cross flow

4 Two-Pump Intake

Since the inviscid flow simulations for the single-pump intake showed good agreement with experiments away from the walls, simulations were extended to the two-pump intake geometry. This required restructuring of each subroutine of the main code and generating the computational grid as well as an initial estimate of the velocity field in the two-pump intake.

4.1 The Computational Grid

The computational grid for the two-pump intake geometry is depicted in Fig. 7. The intake consisted of a rectangular pump bay with two vertical suction pipes located at the downstream end of the approach channel. The grid was sub-divided into three blocks: Block 1, representing the rectangular channel and the submerged portion of the suction pipes, had $75 \times 83 \times 29$ grid points in the x , y , and z directions, respectively. Blocks 2 and 3, representing the portions of the suction pipes above the free surface, each had $18 \times 18 \times 16$ grid points in the x , y , and z directions, respectively. Systematic grid refinement studies carried out by Ansar (1997) showed that this grid density was sufficient for grid independent solutions.

The inviscid solution for the flow in the two-pump intake was obtained for two cases. Case 1 was such that the total pump discharge, Q , was evenly distributed between the two pipes, i.e., $Q1/Q = Q2/Q = 0.5$, where $Q = Q1 + Q2$. Case 2 was such that Q was split in a 7-to-3 ratio between the two pipes, i.e., $Q1/Q = 0.7$

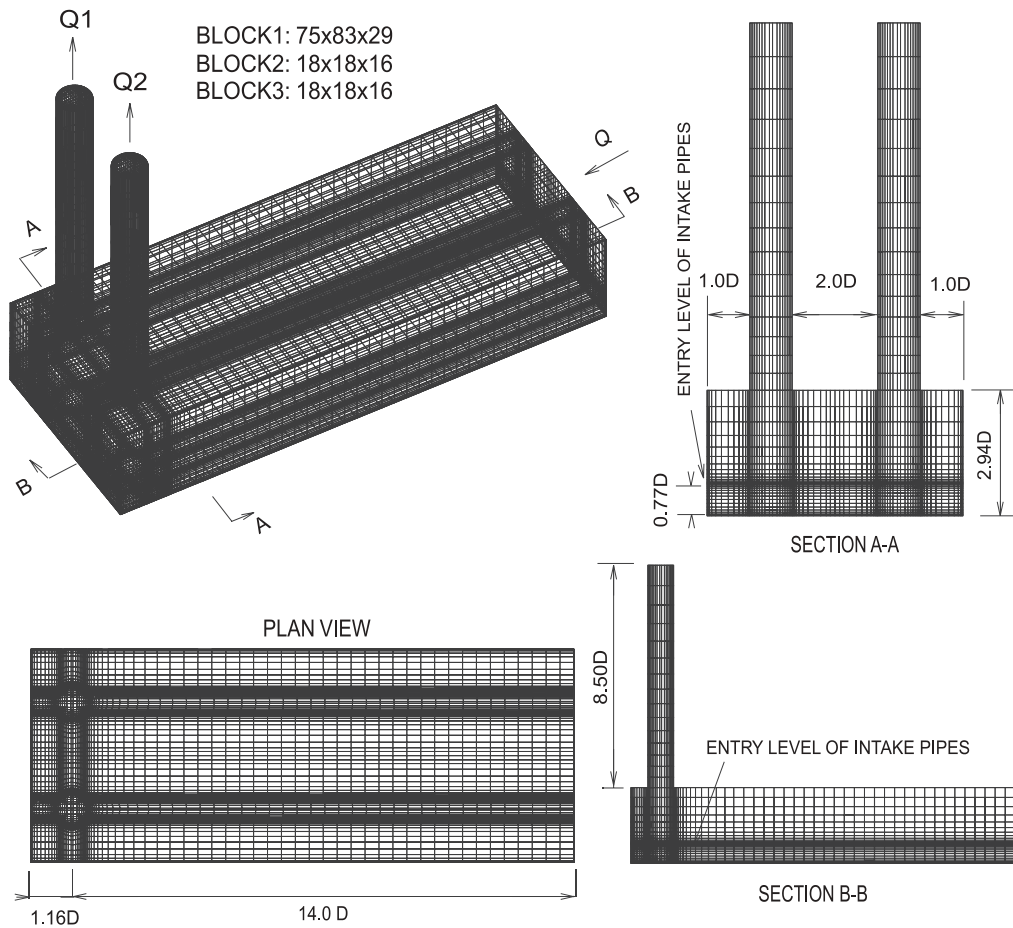


Fig. 7 Computational grid for the two-pump intake

in Pipe 1, and $Q2/Q = 0.3$ in Pipe 2. In a practical sense, Case 2 corresponds to a scenario of a pumping station that has two pumps with different capacities. In both cases, a nearly uniform flow distribution, approximating the well-known logarithmic profile, was used as the upstream boundary conditions. As with the

single-pump intake, slip boundary conditions were imposed at solid boundaries and a symmetry boundary condition was implemented at the free surface.

Figs. 8(a) and 8(b) show stream traces for Case 1 plotted on horizontal planes at the free surface and just below the entry level of

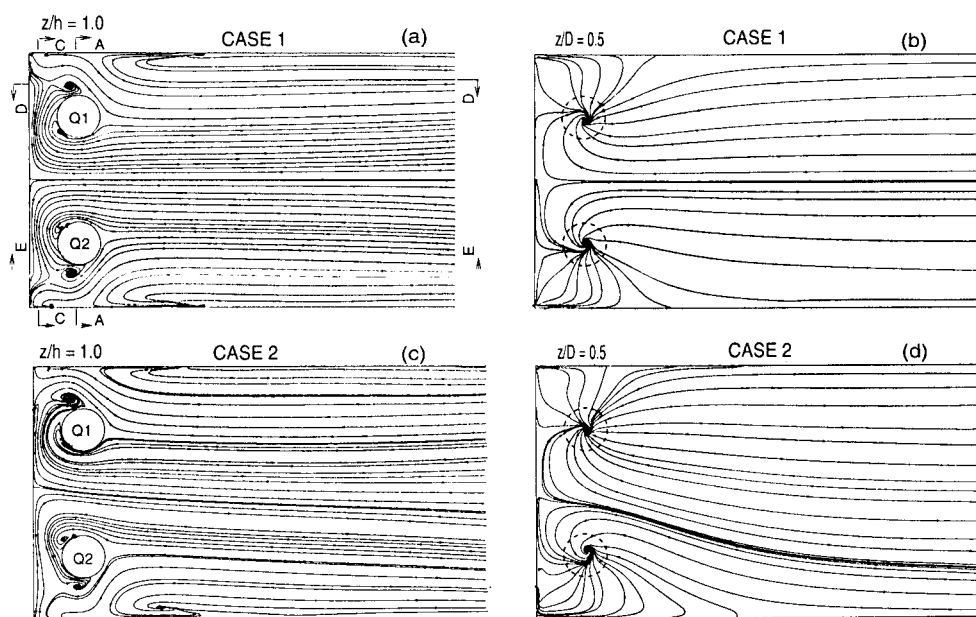


Fig. 8 Inviscid solution for Case 1 [(a) and (b)] and Case 2 [(c) and (d)], showing free-surface vortices at $z/h = 1.0$ and floor-attached vortices observed at $z/D = 0.5$

the suction pipes at $z/D = 0.5$, respectively. The dividing streamline is midway between the two suction pipes, as expected. As opposed to the laminar solution, where no vortical structures were observed (Ansar 1997), a number of vortical structures appeared in the flow. These vortices included free-surface vortices near the suction pipes, as shown in Fig. 8(a), and a strong submerged vortex below each suction pipe, as depicted in Fig. 8(b). Note that in Fig. 8(b), the suction pipes are represented by the circles in broken lines.

Figs. 8(c) and 8(d) show similar stream traces for Case 2 on horizontal planes at the free surface and below the entry level of the suction pipes at $z/D = 0.5$, respectively. In this case, vortices are also present at the free surface, as shown on Fig. 8(c), with a stronger vortex next to Pipe 1. Fig. 8(d) depicts the subsurface vortices below the suction pipes for Case 2. The dividing streamline in this case extends further towards the left sidewall because

of a larger flow in Pipe 1 and a re-distribution of flow velocities due to these flow imbalances.

Figs. 9(a) through 9(d) show the stream traces at Sections A-A and C-C that are defined in Fig. 8(a). These sections lie, respectively, in the transverse plane of symmetry of the pipes and the vertical $y-z$ plane located near the backwall at $x/D = 0.90$. Figs. 9(a) and 9(b), which depict the stream traces for Case 1, show that the dividing streamline near the suction pipes is midway between the two pipes. Fig. 9(a) also shows two longitudinal floor-corner vortices near the sump floor. There are also backwall-attached vortices at a depth near the entry level of the suction pipe, as shown in figure 9(b). Figs. 9(c) and 9(d) show the flow patterns at Sections A-A and C-C for Case 2. In this case, a backwall-attached vortical structure can be seen behind Pipe 1 that carried the larger discharge, as shown on Fig. 9(d).

Figs. 9(e) and 9(f), respectively, show stream traces for Case 1 at

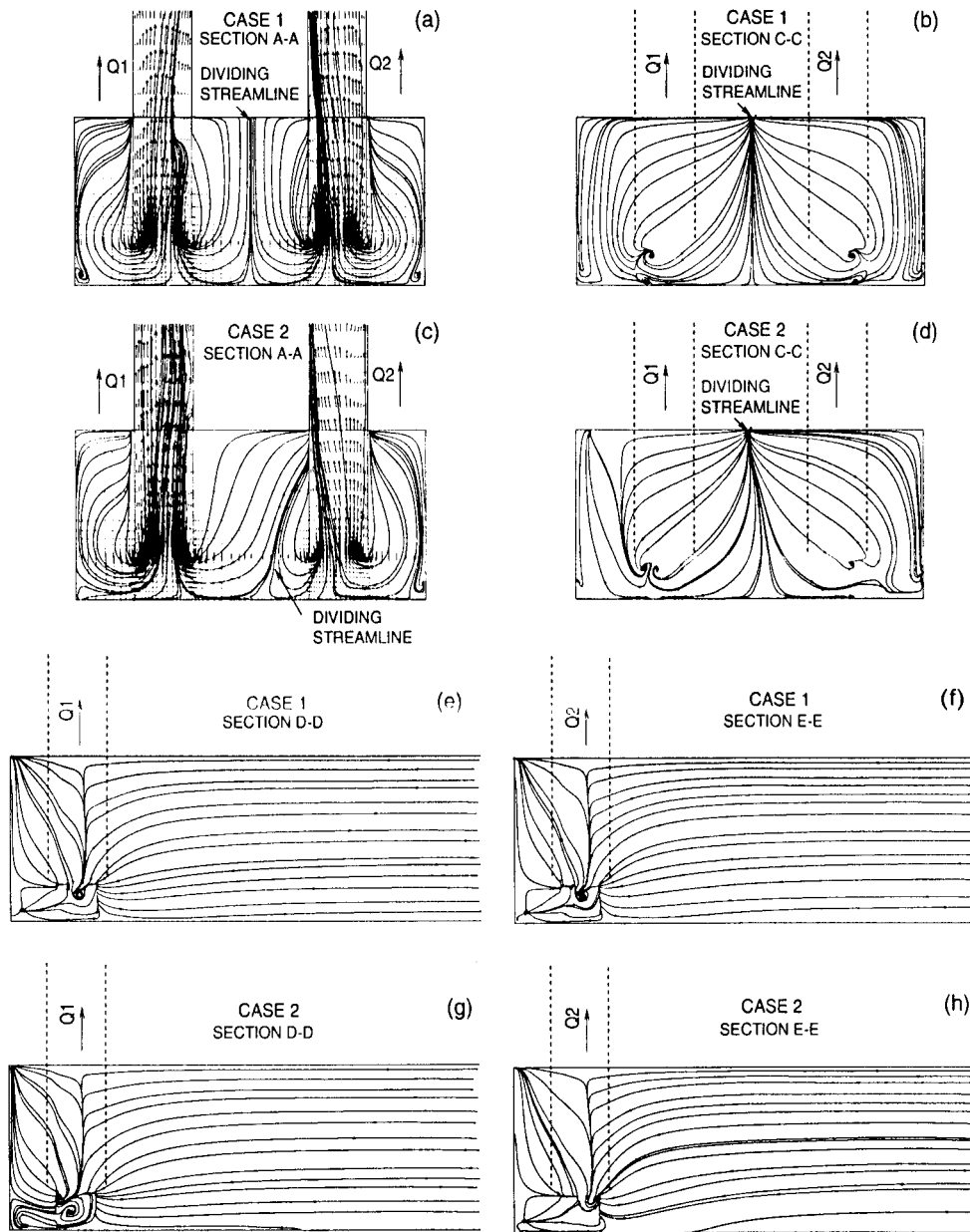


Fig. 9 Inviscid solution for Case 1 [(a), (b), (e) and (f)] and Case 2 [(c), (d), (g) and (h)], showing corner, backwall- and sidewall-attached subsurface vortices

Sections D-D and E-E. These sections are vertical x - z planes in the vicinity of the suction pipes, as shown in Fig. 8(a). These figures are practically identical, with a counterclockwise transverse vortex near the entry level of the suction pipe. This confirms the symmetry of the solution with respect to the longitudinal axis of symmetry of the intake, when the two pipes carried the same discharge.

Figs. 9(g) and 9(h) depict the flow patterns at Sections D-D and E-E for Case 2, respectively. Fig. 9(g) shows a strong sidewall-attached vortex near the entrance of Pipe 1 ($Q1/Q = 0.7$). By contrast, there is a weak vortical structure near Pipe 2 ($Q2/Q = 0.3$), as depicted in Fig. 9(h). This result shows that passing a higher discharge through one of the suction pipes has the same effect as bringing its adjacent sidewall much closer to it, i.e., increasing the strength of sidewall-attached vortices.

5 Discussion

The present study was driven by the need for a more basic understanding of pump-approach flow distributions at water intakes, especially the effects of the approach flow distributions on the formation of vortices near the intake pipe. The study was intended to specifically address the following issues: (a) How reliable is an inviscid solution in predicting approach-flow features at water intakes, including vortex formation? (b) What effects do flow imbalances in the suction pipes have on the formation of vortices in a two-pump water intake? To this effect, inviscid solutions of the three-dimensional flow in a single-pump and two-pump intakes were developed.

The results in the single-pump intake showed a good agreement with laboratory flow measurements obtained using the Acoustic Doppler Velocimeter. The agreement between the inviscid solution and the measurements should not come as a surprise because of the following:

- (i) Numerous studies (Anwar et al. 1978, Hecker 1984; Padmanabhan and Hecker 1984; Odgaard 1986) have shown that, at sufficiently high Reynolds and Weber numbers (Re and We , respectively, greater than about 30,000 and 10,000), the formation of vortices at water intakes is mostly a function of the Froude and the circulation numbers. Both of these parameters appear in the non-dimensional form of the Euler equations (Hecker 1984; Ansar 1997), which are the governing equations of the three-dimensional inviscid flow. In the Euler equations, the Froude number appears in the pressure gradient terms in the vertical direction (Ansar 1997). The circulation number appears in the convective terms if a reference velocity that depends on the circulation is chosen, as shown by Hecker (1984). Therefore, the inviscid solution accounts for the effects of the two most dominant parameters for vortex formations at water intakes, namely the Froude and circulation numbers.
- (ii) The inviscid solution incorporates the effects of vortex filaments stretching, which plays a key role in the formation of vortices, as explained by De Siervi et al. (1982). In fact, the vorticity transport equation in an inviscid flow expresses a balance between the convection of vorticity and the amplifi-

cation of vorticity due to stretching of vortex filaments. This can be seen by taking the curl of the Euler equation, which results in the following equation:

$$U_j \frac{\partial \Omega_i}{\partial x_j} = \Omega_j \frac{\partial U_i}{\partial x_j} \quad (6)$$

where $i, j = 1, 2, \text{ and } 3$ and Ω_i is the component of vorticity in the i -th direction. In equation (6), the left-hand side consists of the convective terms, and the right-hand side, the vortex-stretching terms.

The main point here is that at many water intakes, especially those with a cross-flow, the swirling flow patterns (vortices, re-circulation regions, etc.) are driven to a large extent by the inviscid transport of vorticity, and to a much lesser extent, by turbulence.

- (iii) Yıldırım and Kocabaş (1995) have shown that a potential flow solution predicts the critical submergence depth for free-surface vortices at pump intakes. Critical submergence depth is defined as the depth at which air-entraining vortices start appearing. The potential flow solution is an inviscid solution where the flow is assumed irrotational, i.e., with zero vorticity. As such, it is more restrictive than the inviscid solution described in this paper, where the flow is rotational. Therefore, the inviscid solution that is developed herein should be expected to accurately predict the formation of free-surface vortices.

As expected, the inviscid solution fails to accurately predict the flow in highly viscous-flow regions such as the inside of the suction pipe and the boundary layers on the sump walls. However, the inviscid solution is still a very useful tool for predicting the swirling flow patterns in the vicinity of the suction pipe. As explained earlier, these swirling flow patterns are culpable to pump-operating problems such as vibration, cavitation, and loss of net positive suction head.

The numerical solution in the two-pump intake showed a strengthening of the vortices when there are imbalances of flow between the two suction pipes. This is mostly due to the loss of symmetry in the approach flow, and a greater amplification of vorticity at the suction pipe carrying the higher discharge.

6 Conclusion and Summary

This paper describes the results of the three-dimensional numerical simulations of the inviscid flow in single and two-pump intakes. The inviscid solution in the single-pump intake was compared with laboratory flow measurements obtained using the Acoustic Doppler Velocimeter. The results showed similar free-surface flow patterns between the experiments and the numerical simulations for both the cross-flow and no-cross-flow cases. A good agreement between the computed streamwise velocities and those measured in the experiments was also obtained away from the solid boundaries for both cases.

In the two-pump intake simulations, when the inflow discharge was unevenly split between the suction pipes, the dividing streamline gradually shifted toward the sidewall adjacent to the

pipe carrying the smaller discharge, as one approaches the sump floor. This flow imbalance also resulted in the strengthening of the vortices in the vicinity of the suction pipes.

Based on the results obtained so far, one can envision the following use of the developed code:

- (a) To identify approach flow features that are responsible for swirling flow problems at existing water intakes;
- (b) To determine approach flow distributions and intake layout (backwall, sidewall and floor clearances, suction pipe diameter, etc.) that result in minimal formation of free-surface and subsurface vortices; and
- (c) To reduce the cost associated with conceptual and final design of a large pumping station by reducing the number of design scenarios to test in a small-scale laboratory model, or by eliminating altogether the need for a physical model.

Acknowledgement

This study was conducted under the Electric Power Research Institute (EPRI) Tailored Collaboration Program. It was sponsored by EPRI and Iowa's three investor-owned electric utilities: IES Utilities, Interstate Power, and Mid-American Energy Company. The authors are thankful to Prof. V.C. Patel, Director of the Iowa Institute of Hydraulic Research, The University of Iowa, for his keen interest in the subject and his thoughtful inputs given throughout the study.

Notations

The following symbols are used:

Latin Symbols

A_j	Diagonal matrices of the contravariant components of velocity;
b	Pump-bay width (= 61.0 cm);
c	Suction-line floor clearance (= 11.8 cm);
D	Diameter of the suction pipe (= 15.2 cm);
Fr	Froude number;
g	Gravitational acceleration;
h	Pump-approach flow depth (= 47.9 cm);
J	Jacobian of the geometric transformation;
\bar{n}	Unit normal vector;
P	Pressure;
\bar{Q}	Velocity vector defined by $= (U_1, U_2, U_3)^T$;
Q	Discharge through the pump sump;
Q_{main}	Discharge in the main channel;
$Q1$	Discharge in Pipe 1;
$Q2$	Discharge in Pipe 2;
Re	Reynolds number;
T	Temperature;
t	Time;
U	Time-averaged velocity in the streamwise direction;
U_p	Mean axial velocity in the suction pipe;
U^i	Contravariant components of velocity;
We	Weber number;
x	Coordinate in the streamwise direction;

y	Coordinate in the transverse direction; and,
z	Coordinate in the vertical direction.

Greek Symbols

ν	Kinematic viscosity (= 0.00952 cm ² /s);
Ω_i	Component of vorticity in the i -th direction; and
ξ^i	Generalized curvilinear coordinates ($i = 1, 2, \text{ and } 3$).

References

- [1] Ansar, M., and Nakato, T. (1995). 'Effects of Approach Flow on Vortex Formation at a Pump Intake,' *Proceedings of the 26th IAHR Biennial Congress HYDRA 2000*, Vol. 2, London, UK, 11-15 September, pp. 114-119.
- [2] Ansar, M. (1997). 'Experimental and Theoretical Studies of Pump-Approach Flow Distributions at Water Intakes,' *Ph.D. Dissertation*, Iowa Institute of Hydraulic Research, The University of Iowa, Iowa City, Iowa 52242, USA.
- [3] Ansar, M. and Nakato, T. (2001). 'Experimental Study of 3D Pump-Intake Flows With and Without Cross Flow,' *J. of Hydr. Engr.*, ASCE, Vol. 127, No. 10, pp. 825-834.
- [4] Anwar, H.O., Weller, J.A., and Amphlett, M.B. (1978). 'Similarity of Free-Vortex at Horizontal Intake,' *J. of Hydr. Res.*, Vol. 16, No.2, pp. 95-105.
- [5] Bauer, D.I., Nakato, T., and Ansar, M. (1997). 'Vortex Suppression in Multiple-Pump Sumps,' *Proceedings of the 27th IAHR Congress (Theme D)*, San Francisco, California, 10-15 August, pp. 549-554.
- [6] Constantinescu, G., Patel, V.C., Ansar, M., and Nakato, T. (1997). 'Computational Fluid Dynamics Model for Pump-Intake Flow and Users' Guide,' *IIHR Report No. 387*, Iowa Institute of Hydraulic Research, The University of Iowa, Iowa City, Iowa 52242, USA.
- [7] Constantinescu, G., and Patel, V.C. (1997). 'Numerical Simulation of Flow in Pump-Bays Using Near-Wall Turbulence Models,' *IIHR Report No. 394*, Iowa Institute of Hydraulic Research, The University of Iowa, Iowa City, Iowa 52242, USA.
- [8] Constantinescu, G., and Patel, V.C. (1998). 'Numerical Model for Simulation of Pump-Intake Flow and Vortices,' *J. of Hydr. Engrg.*, ASCE, Vol. 124, No. 2, pp. 123-134.
- [9] De Siervi, F., Viguier, H.C., Greitzer, E.M., and Tan, C.S. (1982). 'Mechanisms of Inlet-Vortex Formation,' *J. of Fluid Mech.*, Vol. 124, pp. 173-207.
- [10] Hecker, G.E. (1984). 'Scale Effects in Modeling Vortices,' *IAHR Symposium on Scale Effects in Modeling Hydraulic Structures*, Esslingen am Neckar, Fedral Republic of Germany, 3-6 September, pp. 6.1-1 to 6.1-9.
- [11] Melville, B.W., Ettema, R., and Nakato, T. (1994). 'Review of Flow Problems at Water Intake Pump Sumps,' *EPRI Research Project RP3456-01 Final Report*, Electric Power Research Institute, Palo Alto, California 94304, USA.

- [12] Nakato, T. (1984). 'Model Investigation of Intake-Shoaling and Pump-Vibration Problems: Iowa Generation Council Bluffs Unit 3 Circulating-Water Intake,' *IHR Report No. 283*, Iowa Institute of Hydraulic Research, The University of Iowa, Iowa City, Iowa 52242, USA.
- [13] Nakato, T., and Krütten, M. (1999). 'Coping with Strong Cross Flows at Pump Intake,' *Proceedings of the 28th IAHR Biennial Congress*, Graz, Austria, 22-27 August.
- [14] Odgaard, J.A. (1986). 'Free-Surface Air Core Vortex,' *J. of Hydr. Engrg.*, ASCE, Vol. 112, No. 7, pp. 610-620.
- [15] Padmanabhan, M., and Hecker, G.E. (1984). 'Scale Effects in Pump Sump Models,' *J. of Hydr. Engrg.*, ASCE, Vol. 110, No. 11, pp. 1540-1556.
- [16] Sotiropoulos, F., and Patel, V.C. (1992). 'Flow in Curved Ducts of Varying Cross-Section,' *IHR Report No. 358*, Iowa Institute of Hydraulic Research, The University of Iowa, Iowa City, Iowa 52242 USA.
- [17] Sweeney, C. E., Elder, R. A., and Hay, D. (1982). 'Pump Sump Design Experience: Summary,' *J. of Hydr. Engrg.*, ASCE, Vol. 108, No. 3, pp. 361-377.
- [18] Tullis, J.P. (1979). 'Modeling in Design of Pumping Pits,' *J. of Hydr. Div.*, ASCE, Vol. 105, No. 9, pp. 1053-1063.
- [19] Yıldırım, N., and Kocabaş, F. (1995). 'Critical Submergence for Intakes in Open Channel Flow,' *J. of Hydr. Engrg.*, ASCE, Vol. 121, No. 12, pp. 900-905.